Discriminating basal cell carcinoma from perilesional skin using high wave-number Raman spectroscopy

Annieke Nijssen
Kees Maquelin
Erasmus MC
Center for Optical Diagnostics and Therapy
Department of Dermatology
Rotterdam, The Netherlands

Luis F. Santos
Erasmus MC
Center for Optical Diagnostics and Therapy
Department of Dermatology
Rotterdam, The Netherlands
and
Instituto Superior Téchnico
Department of Materials
Lisbon, Portugal

Peter J. Caspers
Tom C. Bakker Schut
Erasmus MC
Center for Optical Diagnostics and Therapy
Department of Dermatology
Rotterdam, The Netherlands
E-mail: p.caspers@erasmusmc.nl

Jan C. den Hollander
Erasmus MC
Department of Pathology
Rotterdam, The Netherlands

Martino H. A. Neumann
Gerwin J. Puppels
Erasmus MC
Center for Optical Diagnostics and Therapy
Department of Dermatology
Rotterdam, The Netherlands

Abstract. An expanding body of literature suggests Raman spectroscopy is a promising tool for skin cancer diagnosis and *in-vivo* tumor border demarcation. The development of an *in-vivo* diagnostic tool is, however, hampered by the fact that construction of fiber optic probes suitable for Raman spectroscopy in the so-called fingerprint region is complicated. In contrast, the use of the high wave-number region allows for fiber optic probes with a very simple design. We investigate whether high wave-number Raman spectroscopy (2800 to 3125 cm^{-1}) is able to provide sufficient information for noninvasive discrimination between basal cell carcinoma (BCC) and noninvolved skin. Using a simple fiber optic probe, Raman spectra are obtained from 19 BCC biopsy specimens and 9 biopsy specimens of perilesional skin. A linear discriminant analysis (LDA)-based tissue classification model is developed, which discriminates between BCC and noninvolved skin with high accuracy. This is a crucial step in the development of clinical dermatological applications based on fiber optic Raman spectroscopy. [DOI: 10.1117/1.2750287]

Keywords: skin cancer; Raman spectroscopy; basal cell carcinoma; diagnostic technique; high wave-number region; fiber optic probe.

Paper 06315R received Nov. 6, 2006; revised manuscript received Feb. 27, 2007; accepted for publication Feb. 28, 2007; published online Jun. 22, 2007.

1 Introduction

Basal cell carcinoma (BCC) is the most common cutaneous carcinoma and its incidence is ever increasing.[1–3] Although usually slow growing with an indolent clinical behavior, a minority has an aggressive behavior with significant local destruction. Especially in large carcinomas with an aggressive growth pattern, visual determination of tumor borders can be difficult.[4] Mohs' micrographic surgery is a technique that can identify tumor margins with near 100% certainty, reducing recurrence rates to only 1 to 2%.[5–8] Furthermore, this technique minimalizes the sacrifice of healthy tissue, resulting in smaller tissue defects. This is particularly important since BCCs often appear in the head and neck region. Mohs' micrographic surgery is, however, a laborious method, which is why its use is generally limited to BCCs with an aggressive growth pattern. Novel, less time-consuming techniques are required that enable immediate pre- and intraoperative evaluation of the tumor borders in BCC. Raman spectroscopy is one of the techniques being explored for detection of malignancies and tumor border demarcation.[9–20] It is a spectroscopic technique that provides detailed information concerning the molecular composition of the tissue. Changes in the molecular composition of diseased tissue lead to changes in its Raman spectrum, which can be used to distinguish it from healthy tissue. Gniadecka et al., Sigurdsson et al., and Nunes et al. reported spectral differences between BCC and benign tissue, measuring whole biopsy specimens.[11,13,15] Choi et al. and Short et al. also observed spectral differences between the two tissue types, using confocal Raman spectroscopy.[10,14] Our

Address all correspondence to Annieke Nijssen, Department of Dermatology, Erasmus MC, room Gk 315 - postbus 2040, Rotterdam, Zuid-Holland 3000 CA Netherlands; Tel: 0031-6-4147387; fax: 0031-10-4087671; E-mail. a.nijssen@erasmusmc.nl

1083-3668/2007/12(3)/034004/7/$25.00 © 2007 SPIE

previous Raman mapping study of frozen sections has shown *in vitro* that BCC can be distinguished from its surrounding tissue with high sensitivity and specificity.[12] Raman spectroscopy is an optical technique based on light scattering. The technique requires laser light to be delivered to the tissue and scattered light to be collected from the tissue. In a clinical setting, optical fibers in combination with a compact handheld probe could provide the flexibility and ease of use that is desired by the clinician.[9,21,22]

All of the aforementioned studies made use of "the fingerprint region"; the study of Sigurdsson et al. used spectral information from both the fingerprint and the high wavenumber region for discrimination of BCC.[15] The fingerprint region (~400 to 1800 cm^{-1}) is often used for Raman spectroscopic investigations because of the rich biochemical information content. The main disadvantage of using the fingerprint spectral region in combination with fiber optic Raman spectroscopy is that a strong background signal is generated in the optical fiber. The necessary suppression of this background signal leads to complicated designs of fiber optic probes. Researchers have used approaches ranging from bundles of one or more signal collection fibers around a separate laser-delivery fiber to complex compound optical probes.[9,21,23,24] As a consequence, probes are relatively large and inflexible, expensive, and it is difficult to achieve a reproducible performance.[25]

In contrast, the high wave-number (HWVN) spectral region from 2500 to 3800 cm^{-1} is virtually free of signal contributions from the fused-silica-based optical fibers. This brings the major advantage that fiber optic probes for *in-vivo* applications can have a very simple design, and in their simplest form consist of a single unfiltered optical fiber, which guides laser light to the tissue and also serves to collect scattered light and lead it back to the spectrometer.[26] The use of the HWVN spectral region to discriminate between different tissue structures has been demonstrated in several studies.[27–30] These studies have shown that Raman spectra in this region provide sufficient information to separate tissue structures with a different molecular composition. A recent study on brain tumors and bladder has demonstrated that HWVN Raman spectra contain similar diagnostic information as Raman spectra obtained in the fingerprint region.[29]

The purpose of this study was to evaluate whether the Raman signal in the HWVN region, using a very simple fiber optic probe, could provide sufficient information to distinguish BCC from its surrounding (perilesional) skin tissue. This is a crucial step in the development of clinical dermatological applications based on fiber optic Raman spectroscopy.

2 Materials and Methods

2.1 *Sample Preparation*

Tissue specimens were obtained with permission from the Medical Ethics Review Board of the Erasmus University Medical Center Rotterdam. Excised specimens from 19 histologically proven BCC were obtained from 17 individuals from the outpatient clinic of the dermatology department. In all cases, a biopsy was taken from the center of the tumor, in nine cases another biopsy was taken from perilesional skin. The biopsies were placed onto a gauze drenched in physiological NaCl solution (0.9%). Raman measurements were performed on fresh biopsies, without further pretreatment of the samples.

2.2 *Reference Spectra*

Reference spectra were obtained from collagen type 1 (ICN Biochemicals Incorporated, Aurora, Ohio) bovine serum albumin (BSA), oleic acid, palmitic acid, and DNA (Sigma, Zwijndrecht, The Netherlands). These compounds were used without further purification. Collagen was measured in dry state. DNA was dissolved in demineralized water prior to the measurements.

2.3 *Raman Instrumentation*

The laser source was a tunable titanium:sapphire laser (Spectra-Physics, 3900 S, Mount View, California), emitting at 720 nm and pumped by an argon-ion laser (Coherent Innova 300, Santa Clara, California). Laser light was then coupled into a single fused silica optical fiber, 200 μm in diameter, delivering 100 mW of laser power to the sample. The scattered Raman light was collected through the same fiber and passed through a custom-made chevron-type dielectric filter system, to suppress the elastically scattered light. The Raman signal was then focused into a 1-mm-diam detection fiber (Fiberguide Industries) attached to a modified multichannel dispersive spectrometer (System 100, Renishaw, Wotton under Edge, United Kingdom). The spectrometer was equipped with a thermoelectrically cooled deep-depletion charge-coupled device (CCD) detector.

2.4 *Data Acquisition*

On each biopsy specimen, depending on the size of the biopsy, 3 to 5 different points were selected. The fiber optic probe was placed onto the specimen, perpendicular to the surface of the biopsy and at each point six Raman spectra were acquired. To investigate the influence of signal collection time—the signal-to-noise ratio improves with the square root of the signal collection time—on the prediction, the measurements were performed using 10 and 60 sec respectively. In addition, two 1-sec spectra were obtained from one sample of BCC and one sample of perilesional skin.

2.5 *Pathology*

After acquisition of Raman spectra, the biopsy specimens were snap frozen in liquid nitrogen. From each of these biopsy specimens, a series of cryosections (6 μm thick) was prepared. Sections were cut perpendicular to the skin surface with a lateral spacing of 100 μm. Cryosections were fixed in formalin and stained in hematoxylin and eosin (HE) for histopathological evaluation by a pathologist specialized in dermatopathology. According to the histopathological examination, Raman spectra were labeled BCC or noninvolved skin. In 10 out of 19 tumor biopsies, all HE stained sections showed BCC, and tumor tissue was apparent in the entire section (eight nodular and two morphea like BCC). The remaining nine biopsy specimens showed BCC in less than half of the stained sections. Because this made it unclear if Raman spectra were obtained from tumor or perilesional tissue, data obtained from these samples were excluded from the study to avoid contamination of the dataset. This resulted in a total of ten tumor specimens and nine perilesional nontumor speci-

mens that were included in the analysis. From seven patients, both a perilesional nontumor and a tumor specimen were present for comparison.

2.6 *Data Analysis*

2.6.1 *Data preprocessing*

All spectral data processing software was programmed in Matlab 6.1 (Mathworks, Natick, Massachusetts), with the PLS-toolbox 2.0 installed (Eigenvector Research Incorporated, Manson, Washington).

The constant background signal contribution originating from optical elements in the laser light delivery pathway was subtracted from all spectra and spectra were corrected for the instrument response using white-light correction.[23,31] The wave-number axis was calibrated using the spectrum of a neon-argon lamp and the Raman spectrum of cyclohexane. Further data preprocessing consisted of 1. calculating the first derivative of the Raman spectra (Savitsky-Golay: five-point filter, second or polynomial), 2. trimming spectra to the spectral range 2800 to 3125 cm^{-1}, and 3. scaling the spectra to standard normal variance scaling, i.e., all spectra have zero mean and unit variance. A first derivative calculation (step 1) was used as a nonsupervised method to minimize the influence of variations in the fluorescent background.

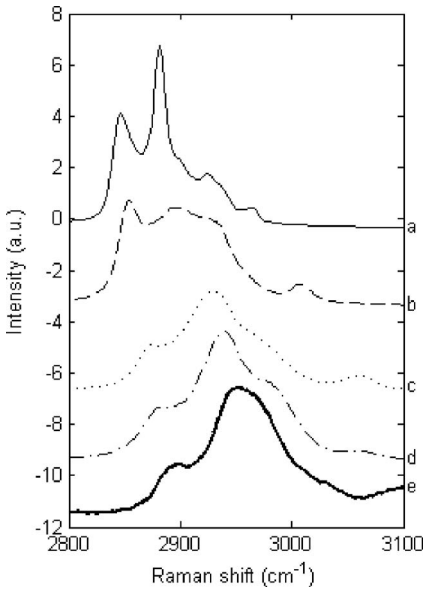

Fig. 1 Reference set of HWVN Raman spectra for spectral fitting: (a) palmitic acid, (b) oleic acid, (c) albumin, (d) collagen, and (e) DNA.

2.6.2 *Least-squares fitting procedure*

A nonrestricted classical least-squares fitting procedure was performed on the 60-sec Raman spectra to acquire information about the chemical composition of BCC and non-BCC tissue. A simple set of model spectra was used to represent the most important molecular constituents of the skin tissues contributing to the overall Raman signal. Raman signals in this study originated predominantly from dermis, with a small contribution of epidermis. The model fit spectra were obtained from BSA and collagen, to represent the dermal and epidermal protein fraction, and oleic acid and palmitic acid as a representation of the dermal and epidermal lipids (Fig. 1, reference set). Since the triple stranded structure of collagen is reflected in a specific Raman spectrum, the more generic protein spectrum of BSA was added to the reference set.

A third-order polynomial was included in the fit to account for small backgrounds in the Raman spectra. To exclude patient-to-patient variation, Raman spectra of both tissue types obtained from the same patient were compared to each other. This (nonrestricted) fitting procedure resulted in positive or negative fit contributions of the reference spectra that point out higher or lower concentrations of the corresponding compounds in the BCC and normal tissue. Relative scattering cross sections were not determined, and therefore all fit coefficients are represented as arbitrary units. Spectral fitting was performed on actual spectra.

2.6.3 *Development of a classification model*

For all 10- and 60-sec Raman spectra, data reduction was performed using principal component analysis (PCA). This is a well-known method for reducing the dimensionality in a dataset.[32] The full set of $n-1$ principal components (PCs) was calculated (n being the number of spectra in the analysis), accounting for 99 to 100% of the total variation in the dataset. A prediction model was developed to classify tissue as normal tissue or BCC, based on their Raman spectrum. The prediction model was based on linear discriminant analysis (LDA), which is a common data classification method. LDA models were developed using only PC scores that represented more than 0.1% variance in the dataset. A two-sided t-test was used to individually select PC scores that showed the highest significance in discriminating the two groups presented. The number of PC scores that was used as an input for an LDA model was kept at least two times smaller than the number of spectra in the smallest model group to prevent overfitting in the LDA model. The prediction accuracy of the identification model was determined by using a "leave-one-patient-out" cross-validation. More details about the LDA procedure can be found in Refs. 9, 33, and 34. The spectra (both benign and malignant) of all but one patient were used to generate the LDA model, which was then used to classify the spectra of the remaining patients. This procedure was repeated for each single patient, providing information about the reproducibility of the method, i.e., whether there is enough discriminating information in the Raman spectra to predict unknown spectra correctly.

LDA classification calculates the probability that a given measurement belongs to each of the classes in the classification model. In our case, this means for each measurement two probabilities were calculated: the probability that the measurement was from noninvolved tissue and the probability that the measurement was from BCC. Any random prediction would yield a 50% probability that a measurement is from either group (BCC and non-BCC). To prevent uncertain prediction where the probabilities are, for instance, respectively 49 and 51%, we introduced a threshold of 70%. Predicted spectra with probability less than 70% were classified as undefined. Separate classification models were constructed for spectra measured in respectively 10 and 60 sec.

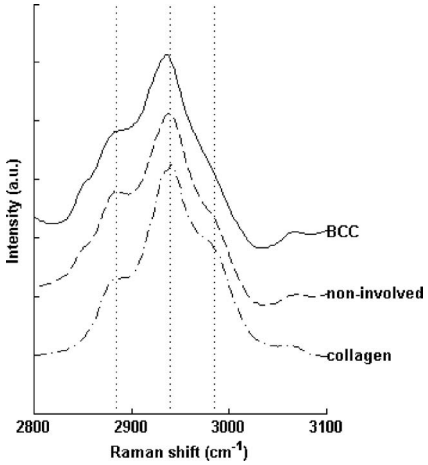

Fig. 2 Comparison of Raman spectra of perilesional skin, BCC, and collagen in the high wave-number region. Dashed lines indicate bands in the noninvolved skin spectrum that can be attributed to collagen: BCC (basal cell carcinoma) (solid line), noninvolved (dashed line), and collagen (dash-dotted line).

3 Results

3.1 *Qualitative Analysis*

Raman spectra obtained from BCC specimens (Fig. 2, line 1) resemble Raman spectra obtained from perilesional skin (Fig. 2, line 2). Both spectra were measured on tissue from the same patient, yet subtle but significant differences can be discerned. The Raman spectrum of noninvolved tissue is almost identical to the Raman spectrum of collagen (Fig. 2, line 3), both spectra exhibiting a distinct peak at 2884 and 2940 cm^{-1} and a shoulder around 2985 cm^{-1}. The Raman spectrum of BCC, exhibiting a peak at 2936 cm^{-1} and a shoulder around 2885 cm^{-1}, shows less resemblance to the collagen spectrum. A more objective way of displaying the differences in chemical composition between perilesional skin and BCC is shown in Fig. 3. This figure shows the relative contributions of the reference spectra to BCC and perilesional skin, respectively. Calculations were performed on all 60s-Raman spectra obtained from the tissue of seven patients, of which both spectra of involved and noninvolved were obtained. One patient was considered an outlier based on spectral characteristics and was not included. The residual of the fit, i.e., the spectrum minus its model fit, exhibits only minor spectral features. This indicates that, to the first-order approximation, the chosen reference set accurately modeled the BCC and noninvolved tissue spectra. Adding DNA to the reference set did not diminish the residual of the fit. Figure 3 shows that both BCC spectra and noninvolved skin spectra are for the greater part made up of protein; the collagen-albumin ratio, however, differs for both tissue types. In all patients, noninvolved skin spectra showed a higher amount of collagen compared to BCC spectra; in four patients this difference was significant. In contrast, the fits of

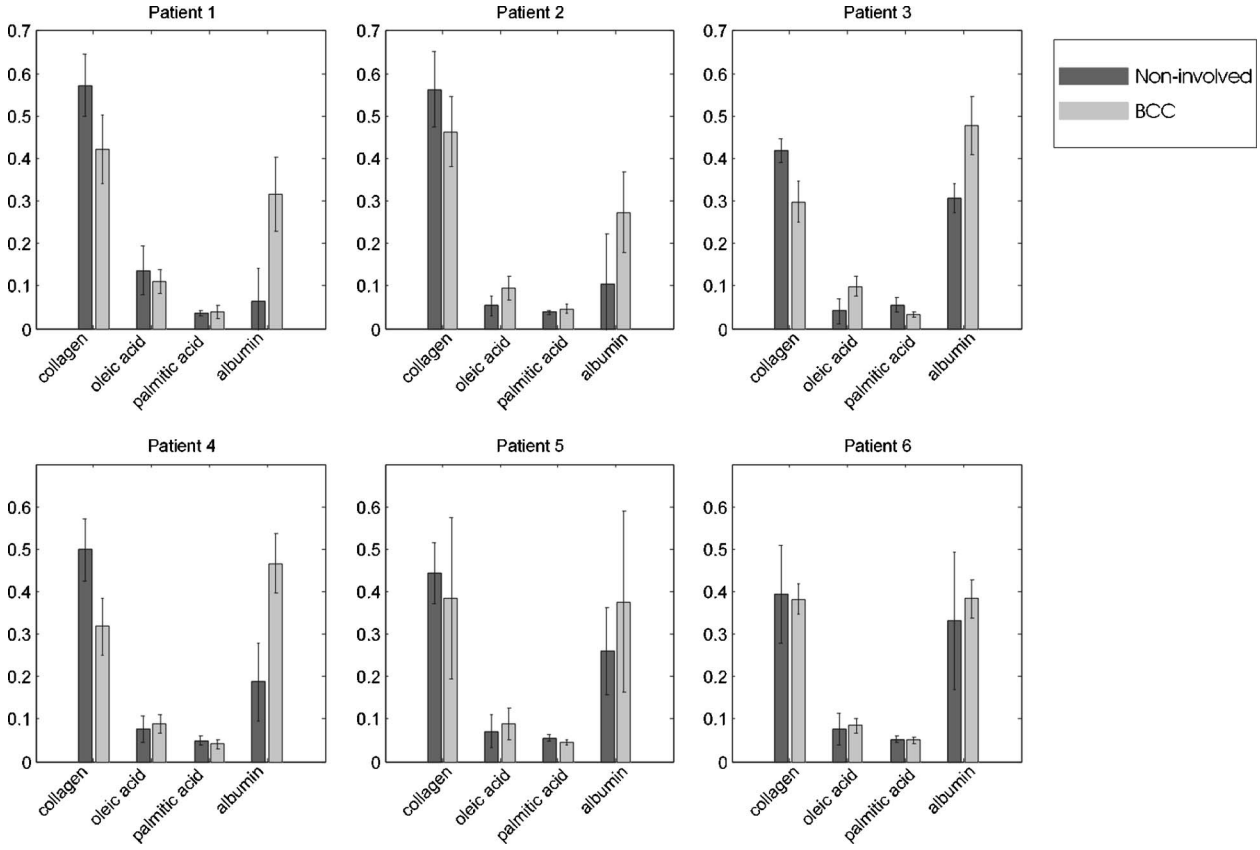

Fig. 3 Fit contributions of BCC and noninvolved skin spectra. There is a marked difference between the contributions of collagen and albumin to BCC and noninvolved skin spectra. BCC spectra of all six patients exhibit a higher contribution of albumin, while noninvolved skin spectra of all six patients exhibit a higher amount of collagen.

Table 1 Results of the classification model based on 10-sec Raman spectra. The performance of this LDA-based classification model was tested by means of a leave-one-patient-out cross-validation; predictions with a probability less than 70% were excluded. In this model 70% of the BCC spectra and 55% of the noninvolved spectra could be predicted.

Raman	BCC	Noninvolved
Pathology		
BCC	100%	0%
Noninvolved	7%	93%

BCC spectra showed a higher contribution of the albumin spectrum. This difference was significant in five out of six patients. BCC spectra and noninvolved skin spectra showed varying amounts of fatty acids in the fit.

3.2 *Classification of Raman Spectra*

A total of 504 Raman spectra (252 BCC and 252 noninvolved, based on histopathological classification) was used as input for the development of two separate LDA-based classification models based on spectra obtained with 10- and 60-sec acquisition time, respectively. A leave-one-patient-out cross-validation resulted in a correct prediction of all (100%) BCC spectra for both signal collection times. For noninvolved skin, 93% of the 10-sec spectra and 99% of the 60-sec spectra were predicted correctly (Tables 1 and 2). Figure 4 shows a Raman spectrum of BCC and noninvolved skin obtained in 1, 10, 60 sec, respectively. The 60-sec spectra exhibited a slightly better signal-to-noise ratio than the 10-sec Raman spectra. Although the lower signal-to-noise ratio in the 1-sec Raman spectra is evident, the spectra still show the characteristic features of BCC and noninvolved skin.

Table 2 Results of the classification model based on 60-sec Raman spectra. The performance of this LDA-based classification model was tested by means of a leave-one-patient-out cross-validation; again, predictions with a probability less than 70% were excluded. Compared to the 10-sec model, this model yielded a higher prediction accuracy; furthermore, a significantly higher number of Raman spectra (95% of the BCC spectra and 81% of the noninvolved skin spectra) could be predicted.

Raman	BCC	Noninvolved
Pathology		
BCC	100%	0%
Noninvolved	1%	99%

4 Discussion

We have demonstrated large and consistent differences between the HWVN Raman spectra of BCC and its surrounding noninvolved tissue. Based on 60-sec Raman spectra, BCC and noninvolved tissue could be distinguished with high accuracy. Using a 70% threshold for the probability of prediction, BCC could be detected with 100% certainty and noninvolved tissue with a certainty of 99%.

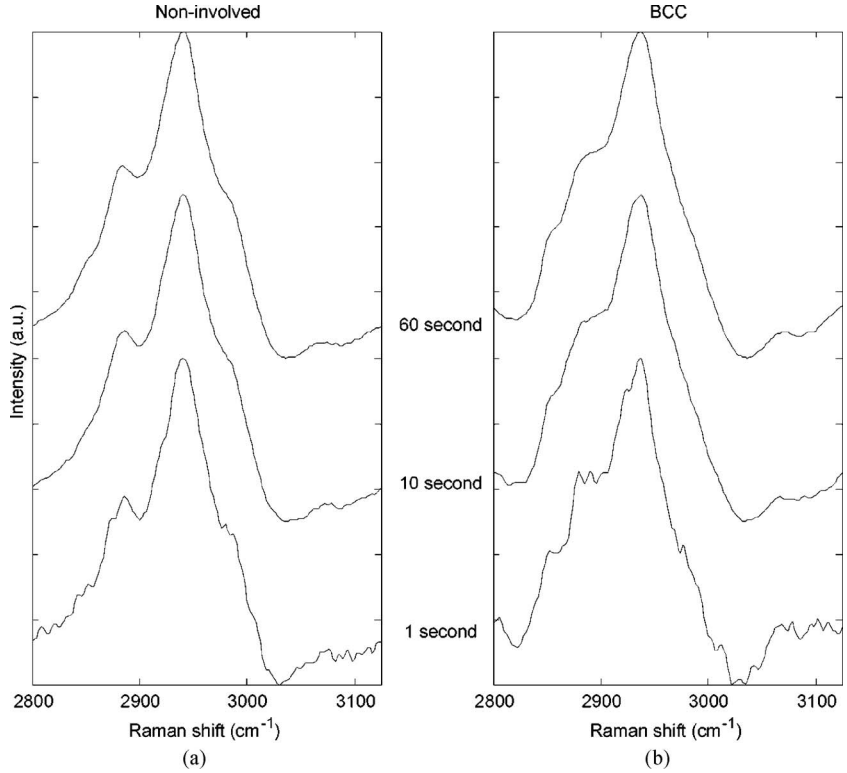

Fig. 4 Comparison of Raman spectra of (a) perilesional skin and (b) BCC obtained in 1, 10 and 60 sec. In both figures a direct correlation between signal-to-noise ratio and signal collection time can be observed.

Although tissue classification is the primary outcome of diagnostic measurements in a clinical setting, understanding the underlying spectral differences that are decisive for these classification results is crucial for further development and validation of the methodology. We therefore analyzed the spectral differences and related these to molecular differences that can be expected between BCC and noninvolved skin. The major discriminating factor could be related to the collagen content. Raman spectra obtained from noninvolved skin biopsies show a strong resemblance to the Raman spectrum of collagen, both spectra exhibiting peaks at the same wave-number shift. This is in accordance with the biochemical composition of the dermis, known to consist of ~70% collagen by dry weight,[35] and is also consistent with the findings of our previous studies using the fingerprint region.[12,36]

Semiquantitative assessment by spectral fitting, which is a more objective method, clearly showed that the collagen content in the BCC sample was significantly lower than in the noninvolved samples. Spectral features of DNA could not be discerned in the BCC spectra. This may be due to the relatively small signal intensity of DNA vibrations in the HWVN Raman spectral region, and because sampling volume in the fiber optic measurements was relatively large. In our previous study and a study by Short et al.—in which specific spectral features of DNA could be detected in BCC spectra—measurements were performed with a confocal Raman microspectrometer, which used a small sampling volume. This enabled detection of localized concentrations of DNA, whereas these local variations would average out in fiber optic measurements. In our previous study, a higher amount of free fatty acids in BCC than in noninvolved tissue was observed. Although in this study, in five of six patients the amount of oleic acid was higher in BCC than noninvolved tissue, this difference was not significant.

The discriminants of the LDA model also provide information about the spectral differences between clusters. The discriminants produced by the LDA strongly resembled the Raman spectrum of collagen, which points to collagen as the major discriminating factor between the two tissue types. This is in agreement with the study by Sigurdsson et al., who reported the wave-number area around 2940 cm^{-1}, which corresponds to collagen being one of the spectral regions containing discriminative information between BCC and noninvolved tissue. In this study, discrimination of BCC was based on spectral information from both the high wave-number region and the fingerprint region.

The use of LDA as a classification method has specific advantages for clinical applications. To separate the two groups of Raman spectra, a prediction model was constructed with a 70% probability cutoff point (see Materials and Methods in Sec. 2). In a clinical setting, this would imply that a measurement results in one of the three classifications: tumor, non-tumor, or undefined. Using the LDA approach, classification can be done automatically and in real time. This enables the clinician to immediately repeat a measurement in case of an "undefined" classification. An important factor for clinical applicability of Raman-based diagnostics is speed or signal collection time. Increasing signal collection time improves the signal-to-noise ratio of the spectrum. Tables 1 and 2 show that increasing the signal collection time from 10 to 60 sec results in an improvement in specificity from 93 to 99%. At the same time, a dramatic decrease is seen in the number of predictions that are below the probability cutoff of 70%; 95 out of 252 of the 10-sec spectra versus 31 out of 252 of the 60-sec spectra could not be predicted with a probability higher than 70%. This shows that with the current equipment, the signal-to-noise ratio is suboptimal, in which case the effect on the prediction accuracy of the method is greatly reduced by the incorporation of a probability threshold of 70%, which adds to the robustness of the classification method.

In this exploratory study, we used Raman spectra obtained in both 10 and 60 sec to distinguish BCC from noninvolved tissue. We also collected several 1-sec Raman spectra from both tissue types. Figure 4 shows a Raman spectrum of BCC and noninvolved skin obtained in all three signal collection times. Although a lower signal-to-noise ratio in the 1-sec Raman spectra is evident, the spectrum still shows the characteristic spectral features of BCC and noninvolved skin. Optimization of the equipment will lead to an increase in signal detection efficiency and shorter collection times in the future.

For the first time exclusively, the high wave-number shift region was employed in a Raman spectroscopic study on BCC. By incorporating a threshold for the probability of prediction in the classification model, tumor tissue could be distinguished with a 100% prediction accuracy and noninvolved tissue with a 99% prediction accuracy. This demonstrates that diagnostic information extracted from the HWVN spectral region can compete with that extracted from the fingerprint region. The major advantage of HWVN Raman spectroscopy as compared to fingerprint Raman spectroscopy is the absence of a strong interfering background signal from optical fibers, which can be a major obstacle for fiber optic Raman applications using the fingerprint spectral region. The absence of this background enables much simpler and smaller fiber optic probes. For instance, the HWVN probe in this study consisted of one single, unfiltered optical fiber, which was used for both delivery and collection of the laser light.

Mohs' micrographic surgery is a very accurate technique, but it is very laborious with low patient throughput and is therefore expensive. A fast and noninvasive tool for diagnosing the tumor borders in BCC, based on HWVN Raman spectroscopy, has great potential to speed up the Mohs' surgical procedure. This would facilitate a widespread use of Mohs' micrographic surgery.

References

1. S. A. Holmes, K. Malinovsky, and D. L. Roberts, "Changing trends in non melanoma skin cancer in South Wales," *Br. J. Dermatol.* **143**, 1224–1229 (2000).
2. A. A. Demers, Z. Nugent, C. Mihalcioiu, M. C. Wiseman, and E. V. Kliewer, "Trends of non melanoma skin cancer from 1960 through 2000 in a Canadian population," *J. Am. Acad. Dermatol.* **53**, 320–328 (2005).
3. L. J. Christenson, T. A. Borrowman, C. M. Vachon, M. M. Tollefson, C. C. Otley, A. L. Weaver, and R. K. Roenigk, "Incidence of basal cell and squamous cell carcinomas in a population younger than 40 years," *J. Am. Med. Assoc.* **294**, 681–690 (2005).
4. E. Epstein, "How accurate is the visual assessment of basal cell carcinoma margins?" *Br. J. Dermatol.* **89**, 37–43 (1973).
5. N. W. Smeets, G. A. Krekels, J. U. Ostertag, B. A. Essers, C. D. Dirksen, F. H. Nieman, and H. A. M. Neumann, "Surgical excision vs Mohs' micrographic surgery for basal cell carcinoma of the face: randomised controlled trial," *Lancet* **364**, 141–147 (2004).
6. D. E. Rowe, R. J. Caroll, and C. L. Day, "Mohs surgery is the treatment of choice for recurrent (previously treated) basal cell carci-

noma," *J. Dermatol. Surg. Oncol.* **15**, 424–431 (1989).
7. M. R. Thissen, M. H. Neumann, and L. J. Schouten, "A systematic review of treatment modalities for primary basal cell carcinomas," *Arch. Dermatol.* **135**, 1177–1183 (1999).
8. D. E. Rowe, R. J. Carroll, and C. L. Day, "Long-term recurrence rates in previously untreated (primary) basal cell carcinoma: implications for patient follow-up," *J. Dermatol. Surg. Oncol.* **15**, 315–328 (1989).
9. T. C. Bakker Schut, M. J. H. Witjes, and J. M. Sterenborg, "In vivo detection of dysplastic tissue by Raman spectroscopy," *Anal. Chem.* **72**, 6010–6018 (2000).
10. J. Choi, J. Choo, H. Chung, D. G. Gweon, J. Park, H. J. Kim, S. Park, and C. H. Oh, "Direct observation of spectral differences between normal and basal cell carcinoma (BCC) tissues using confocal Raman microscopy," *Biopolymers* **77**, 264–272 (2005).
11. M. Gniadecka, H. C. Wulf, N. Mortensen, and D. H. Christensen, "Diagnosis of basal cell carcinoma by Raman spectroscopy," *J. Raman Spectrosc.* **28**, 125–129 (1997).
12. A. Nijssen, T. C. Bakker Schut, F. Heule, P. J. Caspers, D. P. Hayes, M. H. Neumann, and G. J. Puppels, "Discriminating basal cell carcinoma from its surrounding tissue by Raman spectroscopy," *J. Invest. Dermatol.* **119**, 64–69 (2002).
13. L. D. Nunes, A. A. Martin, L. Silviera, and M. Zampieri, "FT-Raman spectroscopy study for skin cancer diagnosis," *Spectroscopy (Eugene, Or.)* **17**, 597–602 (2003).
14. M. A. Short, D. I. Mc Lean, H. Zeng, A. Alajan, and X. K. Chen, "Changes in nuclei and peritumoral collagen within nodular basal cell carcinomas via confocal micro-Raman spectroscopy," *J. Biomed. Opt.* **11**(3), 34004 (2006).
15. S. Sigurdsson, P. A. Philipsen, L. K. Hansen, J. Larsen, M. Gniadecka, and H. C. Wulf, "Detection of skin cancer by classification of Raman spectra," *IEEE Trans. Biomed. Eng.* **51**, 1784–1793 (2004).
16. M. V. Chowdary, K. K. Kumar, J. Kurien, S. Mathew, and C. M. Krishna, "Discrimination of normal, benign and malignant breast tissues by Raman spectroscopy," *Biopolymers* **83**, 556–569 (2006).
17. P. Crow, B. Barrass, C. Kendall, M. Hart-Prieto, M. Wright, R. Persad, and N. Stone, "The use of Raman spectroscopy to differentiate between prostatic adenocarcinoma cell lines," *Br. J. Cancer* **92**, 2166–2170 (2005).
18. A. S. Haka, Z. Volynskaya, J. A. Gardecki, J. Nazemi, J. Lyons, D. Hicks, M. Fitzmaurice, R. R. Dasari, J. P. Crowe, and M. S. Feld, "In vivo margin assessment during partial mastectomy breast surgery using Raman spectroscopy," *Cancer Res.* **66**, 3317–3322 (2006).
19. S. Koljenovic, T. B. Schut, A. Vincent, J. M. Kros, and G. J. Puppels, "Detection of meningioma in dura mater by Raman spectroscopy," *Anal. Chem.* **77**, 7958–7965 (2005).
20. D. P. Lau, Z. Huang, H. Lui, C. S. Man, K. Berean, M. D. Morrison, and H. Zeng, "Raman spectroscopy for optical diagnosis in normal and cancerous tissue of the nasopharynx – preliminary findings," *Lasers Surg. Med.* **32**, 210–214 (2003).
21. U. Utzinger, D. L. Heintzelmann, and A. Mahadevan-Jansen, "Near-infrared Raman spectroscopy for in vivo detection of cervical precancers," *Appl. Spectrosc.* **55**, 955–959 (2001).
22. A. Mahadevan-Jansen, M. F. Mitchell, and N. Ramanujam, "Development of a fiberoptic probe to measure NIR Raman spectra of cervical tissue in vivo," *Photochem. Photobiol.* **68**, 427–431 (1998).
23. R. Wolthuis, T. C. Bakker Schut, P. J. Caspers, H. P., J. Buschman, T. J. Römer, H. A. Bruining, and G. J. Puppels, "Raman spectroscopic methods for *in vitro* and *in vivo* tissue characterization," Chap. 32 in *Fluorescent and Luminescent Probes for Biological Activity*, 2nd ed., W. T. Mason, Ed., pp. 433–455, Academic Press, London (1999).
24. H. P. Buschman, E. T. Marple, and M. L. Wach, "In vivo determination of the molecular composition of the artery wall by intravascular Raman spectroscopy," *Anal. Chem.* **73**, 3915–3920 (2000).
25. I. A. Boere, T. C. B. Schut, J. van den Boogert, R. W. F. de Bruin, and G. J. Puppels, "Use of fiber optic probes for detection of Barrett's epithelium in rat esophagus by Raman spectroscopy," *Vib. Spectrosc.* **32**, 47–55 (2003).
26. L. F. Santos, R. Wolthuis, S. Koljenovic, R. M. Almeida, and G. J. Puppels, "Fiberoptic probes for in vivo Raman spectroscopy in the high-wavenumber region," *Anal. Chem.* **77**, 6747–6752 (2005).
27. P. J. Caspers, G. W. Lucassen, E. A. Carter, H. A. Bruining, and G. J. Puppels, "In vivo confocal Raman microspectroscopy of skin: noninvasive determination of molecular concentration profiles," *J. Invest. Dermatol.* **116**, 434–442 (2001).
28. S. W. E. van de Poll, A. Moelker, R. Wolthuis, P. M. T. Pattynama, A. van der Laarse, and G. J. Puppels, "Chemical characterization of atherosclerotic plaque by high-wavenumber Raman spectroscopy," (submitted for publication).
29. S. Koljenovic, T. C. Bakker Schut, R. Wolthuis, B. de Jong, L. Santos, P. J. Caspers, J. M. Kros, and G. J. Puppels, "Tissue characterization using high wavenumber Raman spectroscopy," *J. Biomed. Opt.* **10**(3), 031116 (2005).
30. R. Wolthuis, M. van Aken, K. Fountas, J. S. Robinson, Jr., H. A. Bruining, and G. J. Puppels, "Determination of water concentration in brain tissue by Raman spectroscopy," *Anal. Chem.* **73**, 3915–3920 (2001).
31. G. J. Puppels, W. Colier, J. H. F. Olminkhof, C. Otto, F. F. M. deMul, and J. Greve, "Description and performance of a highly sensitive confocal Raman spectrometer," *J. Raman Spectrosc.* **22**, 217–225 (1991).
32. I. T. Jollife, *Principal Component Analysis*, Springer-Verlag, New York (1986).
33. K. Maquelin, L. P. Choo-Smith, H. P. Endtz, H. A. Bruining, and G. J. Puppels, "Rapid identification of Candida species by confocal Raman microscopy," *J. Clin. Microbiol.* **40**, 594–600 (2002).
34. M. Stone, "Cross-validatory choice and assessment of statistical predictions (with discussion)," *J. R. Stat. Soc. Ser. B (Methodol.)* **36**, 111–147 (1974).
35. H. R. Jakubovic and A. B. Ackerman, "Structure and function of the skin: development, morphology and physiology," Chap. 1 in *Dermatology*, S. L. Moschella and H. J. Hurley, Eds., pp. 3–87, W. B. Saunders Co., Philadelphia (1992).
36. P. J. Caspers, G. W. Lucassen, R. Wolthuis, H. A. Bruining, and G. J. Puppels, "*In vitro* and *in vivo* Raman spectroscopy of human skin," *Biospectroscopy* **4**, S31–39 (1998).